

Mass transport of adsorbates near a discontinuous structural phase transition

E. Granato^{1,2}, S.C. Ying², K.R. Elder^{3,4}, T. Ala-Nissila^{2,4}

¹*Laboratório Associado de Sensores e Materiais, Instituto Nacional de Pesquisas Espaciais, 12227-010 São José dos Campos, São Paulo, Brazil*

²*Department of Physics, P.O. Box 1843, Brown University, Providence, RI 02912-1843, USA*

³*Department of Physics, Oakland University, Rochester, Michigan 48309-4487, USA and*

⁴*COMP CoE at the Department of Applied Physics,*

Aalto University School of Science, P.O. Box 11000, FI-00076 Aalto, Espoo, Finland

We study the mass transport dynamics of an adsorbed layer near a discontinuous incommensurate striped-honeycomb phase transition via numerical simulations of a coarse-grained model focusing on the motion of domain walls rather than individual atoms. Following an initial step profile created in the incommensurate striped phase, an intermediate hexagonal incommensurate phase nucleates and grows, leading to a bifurcation into two sharp profiles propagating in opposite directions as opposed to broad profiles induced by atomic diffusive motion. Our results are in agreement with recent numerical simulations of a microscopic model as well as experimental observations for the Pb/Si(111) adsorbate system.

I. INTRODUCTION

Recently, there have been extensive studies of both the statics and dynamics of the Pb/Si(111) system¹⁻³. At equilibrium, the system can exist in a striped incommensurate (SI) phase with stripes of domain walls separating commensurate domains, as well as in a hexagonal incommensurate (HI) phase with a hexagonal pattern of domain walls³. In growth processes, the system displays spontaneous self-organization and height selection of Pb islands beyond the monolayer regime. The most striking feature of this system is that the observed rate of island growth implies a rate of mass transport orders of magnitude faster than that from the usual atomic diffusion mechanism²⁻⁴. Theoretical models⁵⁻⁷ indicate that domain wall motion in an incommensurate phase can provide the basic mechanism for such fast dynamics. This anomalous fast mass transport dynamics was subsequently confirmed in another experimental study following the refilling of a hole region in the adsorbate layer in real time⁸. The results also showed an unexpected bifurcation of the initial step profile into two sharp fronts, with a hexagonal phase in between, propagating in opposite directions at a speed much faster than that due to simple atomic diffusion.

Previously, we performed a molecular dynamics (MD) simulation⁷ study of an atomistic model that admits both the SI and HI phases. We found that for an initial step profile separating a bare substrate region (or a hole) from the rest of the SI phase, the domain wall dynamics leads to a bifurcation of the initial step profile into two interfaces propagating in opposite directions at a superfast speed with a HI phase in between, in agreement with the experimental observation on the Pb/Si(111) system⁸. This theoretical study indicates that there are two central ingredients for the observed anomalous superfast mass transport mechanism with profile bifurcation. The first is the existence of a discontinuous transition between two incommensurate phases such as the SI and the HI phases corresponding to different coverages. The second is the

ability of the SI phase to transform itself rapidly into the HI phase near the boundary of the two phases, and the ultrafast domain wall dynamics in the HI phase with a negligible Peierls pinning barrier. However, the simulation study was limited to relatively small system sizes and short time scales when compared to the experimental systems, and the propagating fronts observed in the simulation studies was not as sharp as the experimentally observed. To overcome the system size and time scale limits and clarify the basic physics behind the observed anomalous mass transport mechanism like the one observed for Pb/Si(111) system, we consider in this work a simple continuous density field description of a strained overlayer by the Phase Field Crystal (PFC) model¹⁰. Unlike the conventional PFC model, which retains density variation at microscopic atomic length scales, here we employ a coarse-grained PFC model where the fundamental length scale corresponds to the separation between the domain walls. Thus the origin of the formation of domains and domain walls due to the competition of lattice mismatch strain energy and the adsorbate-substrate binding energy do not appear explicitly in the model. Instead, a periodic array of domains in the incommensurate phase is built into the model via a preferred length scale that corresponds to the separation between the domain walls. This model allows for both an SI and a honeycomb incommensurate (HoI) phases. There is a discontinuous transition between the SI and the HoI phases. This will lead to the bifurcation of the propagating fronts just as that observed in the Pb/Si(111) system⁸ resulting from the discontinuous SI-HI transition. The PFC model also has negligible conversion barriers between the SI and HoI phases as well as that for the Peierls barrier for the HoI model, which are the other ingredients for the anomalous mass transport mechanism. The main advantage of this simple coarse-grained model is that it allows us to study much larger system sizes and get a clear qualitative physical picture of the mass transport mechanism in these systems.

II. COARSE-GRAINED PHASE-FIELD CRYSTAL MODEL

The long-time dynamics of the adsorbed overlayer in the incommensurate phase is essentially controlled by the nature and interaction of the topological defects that characterize such a phase, which consist of an array of interacting domain walls forming the SI, HI or HoI phases. To model such topological defects in the simplest way, we use a phase-field description, where the physically relevant continuous density field is the adsorbed layer coverage. Phase-field models are based on free-energy functionals, which are constructed by considering symmetries and conservation laws¹¹. In order to take into account the structural changes of the domain-wall structure of the adsorbed layer, we follow the approach of the two-dimensional phase-field crystal model¹⁰, described by the free-energy functional

$$F = \int dx dy \left\{ \frac{1}{2} r (\rho - \rho_o)^2 + \frac{1}{2} (\rho - \rho_o) (\nabla^2 + q_o^2)^2 (\rho - \rho_o) + \frac{1}{4} (\rho - \rho_o)^4 - \rho V(x, y) \right\}, \quad (1)$$

where $\rho(x, y)$ is the density field, $r < 0$ and q_o are effective dimensionless parameters, and ρ_o is a dimensionless reference density. For convenience, we set $\rho_o = 1$ and $q_o = 1$. The fundamental length scale is set by $2\pi/q_o$ which corresponds to the spacing between domain walls. The last term represents a pinning potential $V(x, y)$. Unlike the conventional PFC model¹⁰, where the density field corresponds to the atomic density coarse-grained over vibrational time scales, we consider the present model as described in Eq. (1) as a coarse-grained description of the overlayer, which averages out spatial variations at the microscopic scales, but incorporates the domain wall patterns. The domain walls are light (heavy) for a compressively (tensile) strained adsorbate layer. Correspondingly, for a compressively strained system the regions near maxima in the phase field $\rho(x, y)$ correspond to a commensurate domain, whereas the region around the minima of the density constitute the domain walls. For a tensile strained overlayer, we just need to reverse the interpretation of the maxima and minima of the density as domain walls and commensurate domains, respectively. Note that in this interpretation of the model, there is no atomic spatial resolution, but only the spatial resolution of the domain wall structure. It does incorporate the essential ingredient for fast mass transport with profile bifurcation, which is the existence of a structural phase transition with discontinuity in the density. Just as in the standard PFC model¹⁰, the model of Eq. (1) displays a first-order transition between the SI and HoI phases with light (heavy) domain walls for decreasing (increasing) density.

The main assumption for the dynamics is that the density field $\rho(x, y, t)$ should evolve in time in a way that reduces the total free energy F . Since density field is

conserved, it satisfies the continuity equation

$$\frac{\delta \rho}{\delta t} = -\nabla \cdot \vec{J}, \quad (2)$$

where the current density is given phenomenologically by

$$\vec{J} = -\Gamma \nabla \frac{\partial F}{\partial \rho}, \quad (3)$$

where Γ is a kinetic coefficient setting the fundamental time scale for the domain wall motion. This should be orders of magnitude smaller than the atomic diffusion time scale at low temperatures since it is controlled by the relatively small Peierls energy barrier¹² pinning the domain walls and governing the conversion of the SI phase to the HoI phase, rather than the corrugation of the adsorption potential which controls atomic diffusion. Due to the discontinuous transition described by Eq. (1), the dependence of the current density \vec{J} on the density field ρ does not follow, in general, the usual Fick's law $\vec{J} = -D \nabla \rho$. This is consistent with the behavior found in the experiments for Pb/Si(111), which has been argued⁸ to imply an apparent anomalous diffusion. From Eqs. (2) and (3), the time evolution of ρ is then described by the Cahn-Hilliard dynamic equation¹³

$$\frac{\partial \rho}{\partial t} = \Gamma \nabla^2 \frac{\partial F}{\partial \rho}. \quad (4)$$

III. NUMERICAL RESULTS

The time evolution was determined by numerical integration of the dynamical equation, Eq. (4), on a uniform square grid of size $L_x dx \times L_y dy$ with $dx = dy = \pi/4$ and $L_x = L_y = 256 - 512$, and time steps $dt = 0.05 - 0.1$. Figure 1 shows a portion of the phase diagram near the SI to HoI phase transition as a function of the average density $\bar{\rho}$ (for $V(x, y) = 0$) for the light domain wall case. In the range $\rho_h < \bar{\rho} < \rho_s$, the honeycomb and striped phases coexist while for $\bar{\rho} < \rho_h$ and $\bar{\rho} > \rho_s$, the equilibrium phases correspond to the HoI and SI phases, respectively, as shown in Fig. 2. For small $|r|$ or small $\bar{\rho}$, there is also a uniform phase without domain-wall patterns, which is of no interest here. The time evolution of an initial state with a density profile containing a hole with a lower density ($\rho < \rho_h$) will be different for an initial SI or a HoI phase. For an initial SI phase, the decrease in the average density after creating the hole can bring the system near or into the coexistence region. If the average density $\bar{\rho}$ after the creation of the hole is in the range $\rho_h < \bar{\rho} < \rho_s$, then an HoI region centered at the hole can coexist with the remaining SI phase at long times. For an initial HoI phase, however, the decrease in the density moves the system further away from the coexistence region and there is just a spreading of the density without an expanding interface, following the creation of a hole, eventually tending to a uniform profile.

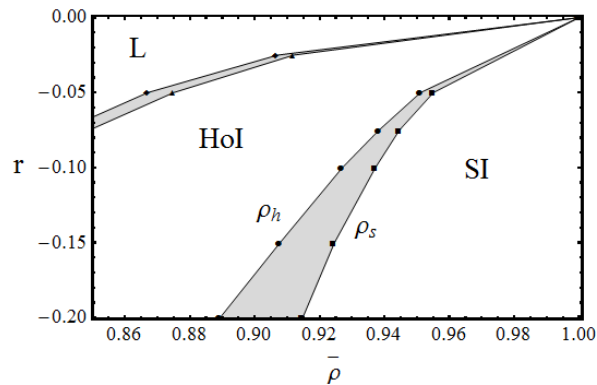


FIG. 1: Phase diagram showing the striped incommensurate phase (SI), honeycomb incommensurate phase (HoI), and the coexistence region (dark area) in the range $\rho_h < \bar{\rho} < \rho_s$. L corresponds to a uniform phase without domain-wall patterns.

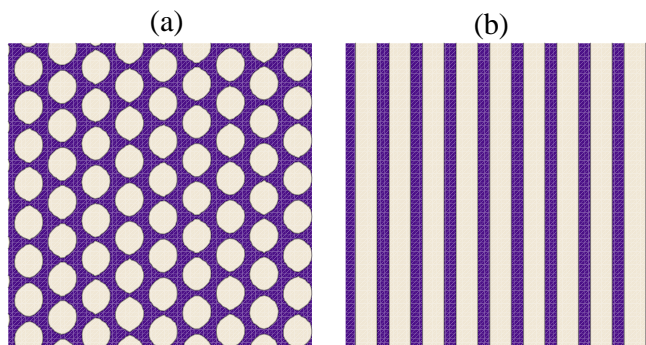


FIG. 2: Domain wall patterns corresponding to the (a) honeycomb incommensurate phase and (b) striped incommensurate phase. The dark areas correspond to domain wall regions where the phase field $\rho(x, y)$ is closest to its minimum value.

We will consider in detail an initial state in the SI phase when the density is higher but close to the coexistence phases boundary ρ_s . From now on we set the parameter $r = -0.1$. In Fig. 3 we show snapshots of the density field for increasing times when a hole with local density $\rho < \rho_h$ is created in an initial striped phase such that the average density $\bar{\rho}$ after the creation of the hole is still higher than ρ_s . An intermediate HoI phase starts to nucleate around the edge of the hole and grows with time, leading to a bifurcation of the initial step profile at edge into two profiles propagating in opposite directions. The outward front corresponds to a SI-HoI interface, where the local stripe pattern is converted into a honeycomb pattern, while the inwards front is a step edge refilling the hole. However, the resulting HoI region decays back into a SI phase for sufficiently long times (Figs. 3e and 3f). As shown in Fig. 4, the time evolution of the radius of the expanding circular interface depends on the density of the initial striped phase, being faster for an initial density closer to the SI-HoI phase boundary, ρ_s , of the coexistence region in the phase diagram of Fig. 1.

For comparison, in Fig. 5 we show the time evolution,

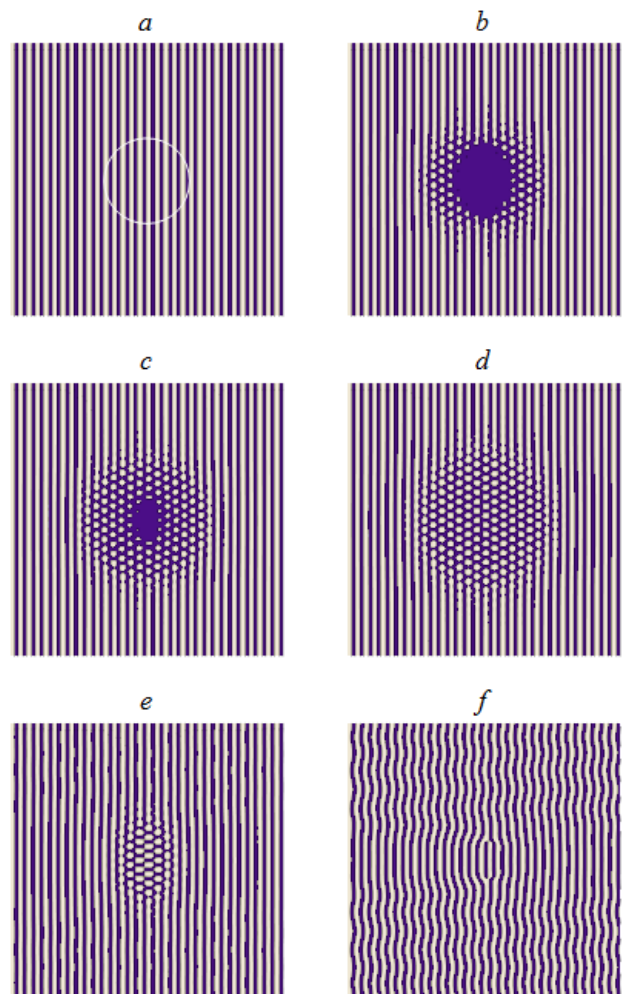


FIG. 3: Snapshots of the density field when a "hole", namely, a circular region of radius $R = 40dx$ (white circle) with an average density $\bar{\rho} = 0.6 < \rho_h$, is introduced in the stripe phase, for increasing times: (a) $t = 0$, (b) $t = 6$, (c) $t = 9$, (d) $t = 21$, (e) $t = 78$, and (f) $t = 126$ in units of $4.8 \times 10^5 dt$. The initial striped phase has an average density of $\bar{\rho} = 0.98$ and $\bar{\rho} = 0.951$ after introduction of the hole.

in the same time interval, when the average density after the introduction of the hole is within the coexistence range, $\rho_h < \bar{\rho} < \rho_s$. Here the HoI region centered at the hole remains at long times.

The nucleation and growth of the intermediate HoI phase in Fig. 3 and the time evolution of the radius of the expanding HoI-SI interface in Fig. 4 are qualitatively consistent with MD simulations of an atomistic model⁷ and with experimental observations for the Pb/Si(111) system⁸. A sign of the decay of the HoI region at long times could be the partial recovery of density in the hexagonal phase found in the experiment. For this system, the boundary of the coexistence region between HoI phase and SI phase, at coverage values ρ_h and ρ_s in Fig. 1, should correspond to the experimentally observed discontinuous jump at the hexagonal-stripe phase boundary

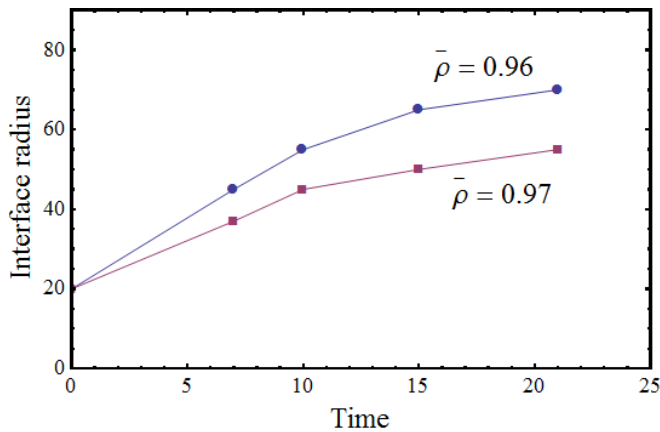


FIG. 4: Radius of the expanding SI-HoI interface as a function of time (in units of $4.8 \times 10^5 dt$) for initial stripe phases with different average densities $\bar{\rho}$, for a hole of radius $R = 20dx$.

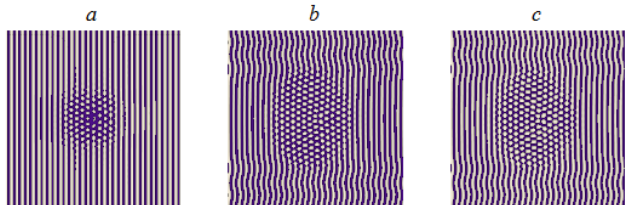


FIG. 5: Snapshots of the density field for increasing times when the average density after introducing a hole with density $\bar{\rho} = 0.8$ is inside the coexistence region. The average density of the initial striped phase is $\bar{\rho} = 0.945$, and $\bar{\rho} = 0.934$ after the introduction of the hole. (a) $t = 4$, (b) $t = 21$, and (c) $t = 126$ in units of $4.8 \times 10^5 dt$.

between coverage $\theta \approx 1.26$ ML and $\theta \approx 1.28$ ML. In this system, fast dynamics are observed experimentally at lower coverages, as long as it exceeds some critical value, $\theta_c \approx 1.24$ ML. The existence of this lower critical coverage for this system is most likely due to the existence of other commensurate phases at or slightly above coverage¹ 1.2 ML. This is beyond the scope of our simple model, which focuses only on the SI and HoI phases near a single commensurate phase at a slightly higher coverage than the SI/HoI boundary. Other more microscopic models^{5,6} can account for this critical coverage as a competition between the lattice mismatch strain energy and the adsorbate-substrate binding energy for increasing coverage.

In the refilling experiment for Pb/Si(111)⁸, the hole is not empty. There is an initial density corresponding to a tightly bound layer of low coverage ($1/3$ monolayer β phase) in the hole, which is only partially equilibrated. To mimic the effect of this partially equilibrated layer, we allow for a random, quenched pinning potential $V(x, y)$ in Eq. (1) localized only inside the hole. We take the simplest model for the random potential, defined by the

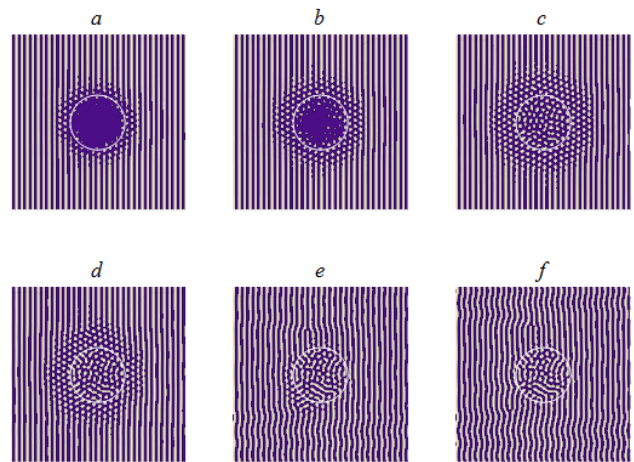


FIG. 6: Snapshots of the density field with quenched disorder inside the hole for increasing times: (a) $t = 5$, (b) $t = 8$, (c) $t = 21$, (d) $t = 42$, (e) $t = 72$, and (f) $t = 126$ in units of $4.8 \times 10^5 dt$. Average density of the initial striped phase is $\bar{\rho} = 0.98$, and $\bar{\rho} = 0.943$ after the introduction of the hole with density $\bar{\rho} = 0.5$. The disorder strength here is $\Delta = 0.08$.

correlations

$$\langle V(x, y)V(x', y') \rangle = \Delta^2 \delta(x - x')\delta(y - y'), \quad (5)$$

where Δ is a measure of the strength of the disorder. As shown in Fig. 6, disorder inside the hole leads to a distorted honeycomb phase inside the hole with structural defects. For holes of sufficiently larger sizes, this should correspond to an amorphous glassy phase even for weak disorder strength¹⁷. Such a phase corresponds to the disordered phase around the inner refilling edge observed experimentally⁸. This leads to a static hexagonal-amorphous interface between the two profiles propagating in opposite directions. However, the hexagonal intermediate phase decays back into the SI phase for sufficiently long times (Fig. 6f). Interesting enough, the amorphous phase inside the hole still remains at such long times.

IV. SUMMARY AND CONCLUSIONS

In this work, we have presented numerical results based on an appropriately coarse-grained PFC model to illustrate the basic physics behind bifurcation of the initial coverage profile in the fast mass transport mechanism observed experimentally^{1-3,8} for the Pb/Si(111) adsorption system. The new model is similar to the traditional PFC model¹⁰, but the interpretation of the phase field and the fundamental length scale are different. It focuses on the domain wall pattern and not the density variation inside the commensurate domains at a microscopic scale. It shares with the conventional PFC model the advantage that numerical work can be performed for

system sizes orders of magnitude larger than in microscopic MD simulation studies⁷. Our results for the mass transport mechanism are qualitatively similar to the previous MD work of an atomistic model⁷. Taken together, they clearly demonstrate that the essential ingredient for the mass transport with a bifurcation of the initial profile is the presence of two incommensurate phases with a first order transition between the two incommensurate phases involving a discontinuity in the coverage. In the work presented here, the two incommensurate phases involved are the SI phase and the HoI phase, but qualitatively it has the same feature as the SI-HI phase transition in the Pb/Si(111) adsorption system. This mass transport mechanism is fast because the HI and the HoI phases have negligible Peierls pinning barriers while the conversion of the SI phase to the HI or HoI phase near the phase transition boundary also involves barriers much lower than those for atomic diffusion. The SI-HI transition corresponds to the Pb/Si(111) adsorption system³ and many heteroepitaxial metallic overlayers¹⁴, while the SI-HoI transition occurs for a system such as Xe/Pt(111),

Xe/Graphite and Kr/Graphite⁹. In these cases, the commensurate state is a $(\sqrt{3} \times \sqrt{3})R30^\circ$ phase, which can undergo a transition into the SI phase and then to the HoI phase^{15,16}. Our results here demonstrate that the phenomena of fast mass transport should not be just confined to the Pb/Si(111) system alone, but is expected to be a general feature for a wide class of surface adsorption systems under appropriate conditions.

Acknowledgments

This work was supported by São Paulo Research Foundation (FAPESP, Grant No. 2014/15372-3) (E.G), CNPq (E.G.), the Watson Institute at Brown University under a Brazil Collaborative Grant (S.-C.Y.) and the National Science Foundation under Grant No. DMR-1506634 (K.R.E.). T.A-N. has been supported in part by the Academy of Finland through its COMP Centre of Excellence Program (projects No. 251748 and No. 284621).

¹ K.L. Man, M.C. Tringides, M.M.T. Loy, and M.S. Altman, Phys. Rev. Lett. **101**, 226102 (2008).

² M.C. Tringides, M. Hupalo, K.L. Man, M.M.T. Loy, and M.S. Altman, In: Michailov, M. (ed.) *Nanophenomena at Surfaces* (Springer, Heidelberg (2011)), pp. 39-65.

³ K. Budde, E. Abram, V. Yeh, and M.C. Tringides, Phys. Rev. B **61**, R10602 (2000); S. Stepanovsky, M. Yakes, V. Yeh, M. Hupalo, and M.C. Tringides, Surf. Sci. **600**, 1417 (2006).

⁴ T.R.J. Bollmann, R. van Gastel, H.J.W. Zandvliet, and B. Poelsema, Phys. Rev. Lett. **107**, 136103 (2011).

⁵ E. Granato and S.C. Ying, Tribol. Lett. **48**, 83 (2012).

⁶ L. Huang, C.Z. Wang, M.Z. Li, and K.M. Ho, Phys. Rev. Lett. **108**, 026101 (2012).

⁷ E. Granato, S.C. Ying, K.R. Elder, and T. Ala-Nissila, Phys. Rev. Lett. **111**, 126102 (2013).

⁸ K.L. Man, M.C. Tringides, M.M.T. Loy, and M.S. Altman, Phys. Rev. Lett. **110**, 036104 (2013).

⁹ L.W. Bruch, R.D. Diehl, and J.A. Venables, Rev. Mod. Phys **79**, 1381 (2007).

¹⁰ K.R. Elder and M. Grant, Phys. Rev. E **70**, 051605 (2004).

¹¹ J.S. Langer, in *Directions in Condensed Matter Physics*, edited by G. Grinstein and G. Mazenko (World Scientific, Singapore, 1986), pp. 165-186.

¹² V.L. Pokrovsky and A.L. Talapov, *Theory of Incommensurate Crystals*, Harwood Academic Publishers. New York (1984).

¹³ J.W. Cahn and J.E. Hilliard, J. Chem. Phys **28**, 258 (1958).

¹⁴ K.R. Elder, G. Rossi, P. Kanerva, F. Sanches, S.C. Ying, E. Granato, C.V. Achim, and T. Ala-Nissila, Phys. Rev. Lett. **108**, 226102 (2012).

¹⁵ S.N. Coppersmith, Daniel S. Fisher, B.I. Halperin, P.A. Lee, and W.F. Brinkman, Phys. Rev. Lett. **46**, 549 (1981).

¹⁶ K.R. Elder, C.V. Achim, E. Granato, S.C. Ying, and T. Ala-Nissila, unpublished.

¹⁷ E. Granato, J.A.P. Ramos, C.V. Achim, J. Lehikoinen, S.C. Ying, T. Ala-Nissila, and K.R. Elder Phys. Rev. E **84**, 031102 (2011).